A&A 489, 1213–1224 (2008)
DOI: 10.1051/0004-6361:200809992

Astronomy & Astrophysics

The γ Doradus CoRoT target HD 49434

I. Results from the ground-based campaign⋆,⋆⋆

K. Uytterhoeven[1,2], P. Mathias[3], E. Poretti[1], M. Rainer[1], S. Martín-Ruiz[4], E. Rodríguez[4], P. J. Amado[4], D. Le Contel[3], S. Jankov[3], E. Niemczura[5,6], K. R. Pollard[7], E. Brunsden[7], M. Paparó[8], V. Costa[4], J.-C. Valtier[3], R. Garrido[4], J. C. Suárez[4], P. M. Kilmartin[7], E. Chapellier[3], C. Rodríguez-López[4], A. J. Marin[4], F. J. Aceituno[4], V. Casanova[4], A. Rolland[4], and I. Olivares[4]

[1] INAF – Osservatorio Astronomico di Brera, via E. Bianchi 46, 23807 Merate, Italy
[2] Instituto de Astrofísica de Canarias, Calle Via Láctea s/n, 38205 La Laguna, Spain
e-mail: katrien@iac.es
[3] UMR 6525 H. Fizeau, UNS, CNRS, OCA, Campus Valrose, 06108 Nice Cedex 2, France
[4] Instituto de Astrofísica de Andalucía (CSIC), Apartado 3004, 18080 Granada, Spain
[5] Institute of Astronomy, KULeuven, Celestijnenlaan 200D, 3001 Leuven, Belgium
[6] Astronomical Institute of the Wroclaw University, ul. Kopernika 11, 51-622 Wroclaw, Poland
[7] Department of Physics and Astronomy, University of Canterbury, Private Bag 4800, Christchurch, New Zealand
[8] Konkoly Observatory, PO Box 67, 1525 Budapest, Hungary

Received 17 April 2008 / Accepted 5 July 2008

ABSTRACT

Context. We present an extensive ground-based photometric and spectroscopic campaign of the γ Dor CoRoT target HD 49434. This campaign was a preparatory step of the CoRoT satellite observations, which occurred between October 2007 and March 2008.
Aims. With satellite data, detection of low-degree pulsation modes only is achievable, and, as no filters are available, with poor identification. Ground-based data promise eventually to identify additional modes and provide extra input for the identification: spectroscopic data allows the detection of high-degree modes and an estimate of the azimuthal number m. We attempt to detect and identify as many pulsation modes as possible from the ground-based dataset of the γ Dor star HD 49434, and anticipate the CoRoT results.
Methods. We searched for frequencies in the multi-colour variations, the pixel-to-pixel variations across the line profiles, and the moments variations in a large dataset, consisting of both multi-colour photometric and spectroscopic data from different observatories, using different frequency analysis methods. We performed a tentative mode identification of the spectroscopic frequencies using the Moment Method and the Intensity Period Search Method. We also completed an abundance analysis.
Results. The frequency analysis clearly indicates the presence of four frequencies in the 0.2−1.7 d^{-1} interval, as well as six frequencies in the 5−12 d^{-1} domain. The low frequencies are typical of γ Dor variables, while the high frequencies are common to δ Sct pulsators. We propose that the frequency 2.666 d^{-1} is the rotational frequency. All modes, for which an identification was possible, appear to be high-degree modes ($3 \leq \ell \leq 8$). We did not find evidence for a possible binary nature of the star HD 49434. The element abundances that we derived are consistent with values obtained in previous analyses.
Conclusions. We classify the γ Dor star HD 49434 as a hybrid pulsator, which pulsates simultaneously in p- and g-modes. This implies that HD 49434 is an extremely interesting target for asteroseismic modelling.

Key words. stars: oscillations – stars: individual: HD 49434 – line: profiles – stars: variables: δ Sct

1. Introduction

We are in a challenging era of asteroseismology. Observers and theoreticians are preparing for the promising output of the CoRoT satellite mission (Baglin et al. 2006), which was launched successfully in December 2006. The CoRoT science programme is twofold. A first goal of the mission involves the detection of extrasolar planets by using the transit method. The asteroseismic goal, on the other hand, aims to probe the internal structures of stars by extracting information from detected pulsation frequencies (several tens, even hundreds, of frequencies, depending on the pulsational class), and, in general, to understand more accurately the process of stellar evolution. To this end, a selection of stars of a wide range of mass, evolutionary status, and spectral type, and belonging to different pulsation classes are monitored.

The CoRoT satellite mission operates in parallel with an enormous observational effort from the ground. Preparatory ground-based observations have not only been a cornerstone

⋆ Based on observations made with ESO Telescopes at the La Silla Observatory under the ESO Large Programme: LP178.D-0361, and on data collected at the Centro Astronómico Hispano Alemán (CAHA) at Calar Alto, operated jointly by the Max-Planck Institut für Astronomie and the Instituto de Astrofísica de Andalucía (CSIC). Also based on observations obtained at Observatorio de Sierra Nevada (Spain), at Observatorio Astronómico Nacional San Pedro Mártir (Mexico), at the Piszkéstetõ Mountain Station of Konkoly Observatory (Hungary), at Observatoire de Haute Provence (France) and at Mount John University Observatory (New Zealand).
⋆⋆ Tables 1, 3 and 9 are only available in electronic form at http://www.aanda.org

in the selection process of suitable targets for asteroseismology (Poretti et al. 2003, 2005), but as the satellite operates in space, simultaneous ground-based observations are critically important to the interpretation of data acquired by the mission. While CoRoT provides high-precision time-series in white light, multi-colour photometry on the ground provides colour information, which allows the identification of the degree ℓ by means of amplitude ratios and phase shifts. High-resolution spectroscopy allows the detection of high-degree modes and the identification of both the degree ℓ and the azimuthal order m by means of, for example, the Moment or Doppler Imaging methods. With the goal of obtaining multi-colour and spectroscopic time-series of a selection of δ Sct, γ Dor, β Cep, and Be CoRoT targets, an extended ground-based campaign, involving both high-resolution spectrographs and multi-colour photometric instruments, were included in the scientific plan of the CoRoT mission (Catala et al. 2006; Uytterhoeven & Poretti 2007; Uytterhoeven et al. 2008).

The γ Dor stars are a challenging class of pulsators for several reasons. The pulsational group has fairly recently been defined (Kaye et al. 1999) and, even though the number of class members is rapidly increasing (more than 130 candidates are known), the number of well-studied cases based on extended time-series is small. Obtaining a good phase coverage from the ground is an observationally challenging task because the intrinsic variations occur with periods of the order of a day (0.4−3 days). Only a few frequencies have been detected so far in individual stars, and amplitudes are fairly small (below 0.05 mag; 2 km s^{-1}). Nevertheless, the γ Dor stars are promising targets for seismic studies because they show g-modes, which can be used to probe the deep interior of the star. Progress has been made in the understanding of the pulsational mechanism, which is probably driven by a flux modulation induced by the upper convective layer (Guzik et al. 2000; Dupret et al. 2004; Grigahcène 2004). However, some details need clarification, such as the thickness and depth of the convection zone and the importance of diffusion.

The γ Dor stars (Spectral type F0V−F2V) occupy an interesting region of the Main-Sequence in the Hertzsprung-Russell (HR-) diagram, being enclosed by the classical instability strip and the instability strip of the solar-like stars. An interesting investigation concerns the presence of hybrid stars, i.e. stars that exhibit both p-mode and g-mode oscillations, in the overlap region of the γ Dor and δ Sct instability strips (Dupret et al. 2005). Observational evidence for self-excited hybrid stars is scarce, and less than a handful genuine hybrid candidates exist, including HD 8801 (Henry & Fekel 2005), HD 114839 (King et al. 2006) and BD+18 4914 (Rowe et al. 2006). The hybrid stars are of particular interest because both the envelope and deep interior of the star can be probed by the study of p-modes and g-modes, respectively.

In this paper, we focus on the ground-based data of the γ Dor star HD 49434 (V = 5.75, F1V). Since HD 49434 is the primary CoRoT target of a 150-days Long Run (LRa1; October 2007−March 2008), several teams performed a detailed study of abundances and fundamental parameters of this star in the preparatory framework of the mission. Summarising their fairly consistent results, we found $T_{\rm eff}$ = 7300 ± 200 K, $\log g$ = 4.1 ± 0.2 dex, [Fe/H] = −0.1 ± 0.2, and $v \sin i$ = 84 ± 5 km s^{-1} (Lastennet et al. 2001; Bruntt et al. 2002, 2004; Mathias et al. 2004; Masana et al. 2006). Gillon & Magain (2006) derived the slightly higher values $T_{\rm eff}$ = 7632 ± 126 K and $\log g$ = 4.43 ± 0.20 dex. We also estimated these parameters from *uvbyβ* and Geneva photometry taken from the GCPD catalogue (*General Catalogue of Photometric Data*,

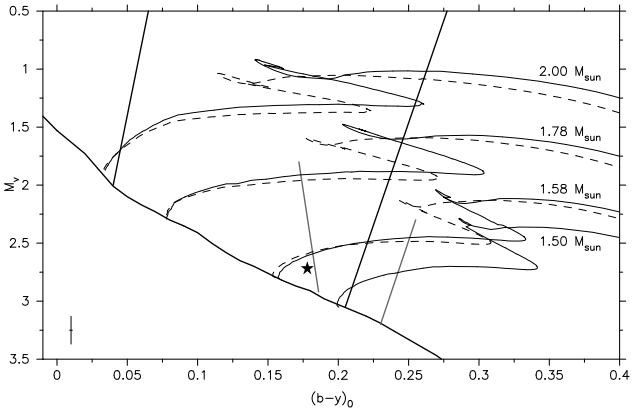

Fig. 1. Colour–magnitude ($(b-y)_0$ versus absolute magnitude M_v) diagram indicating the position of HD 49434 (star). The $(b-y)_0$ and M_v values of HD 49434 (an error bar is given in the left bottom corner) are taken from Hauck & Mermilliod (1998) and from the HIPPARCOS satellite data, respectively. Dashed and solid tracks indicate evolutionary tracks for the overshooting extension distances $d_{\rm over}$ = 0.1 and 0.2, respectively (see Claret 1995, for details). The ZAMS and the borders of the δ Sct (longer black lines) and γ Dor (shorter gray lines) instability strips are indicated by solid lines.

Mermilliod et al. 1997). From the calibration of Napiwotzki et al. (1993), we obtained $T_{\rm eff,[u-b]}$ = 7300 K, $T_{\rm eff,[b-y]}$ = 7230 K, and $\log g$ = 4.1 dex. From the Geneva indices ($B2-V1$), d and $m2$ as proposed by Künzli et al. (1997), we determined $T_{\rm eff}$ = 7200 ± 60 K and $\log g$ = 4.34 ± 0.08 dex. Taking into account all these atmospheric parameters, we adopt effective temperature and surface gravity equal to 7300 K and 4.2 dex, respectively. From 2MASS IR photometry, Masana et al. (2006) estimate an angular semi-diameter of 0.186 ± 0.002 mas, and R = 1.601 ± 0.052 $R_\odot$. An estimate of the mass of HD 49434 M = 1.55 ± 0.14 $M_\odot$ is obtained from evolutionary tracks by Bruntt et al. (2004). A first study of the intrinsic variability of HD 49434 was presented by Bruntt et al. (2002). In a time series of Strömgren data, they found no clear frequencies, but reported a power excess in the frequency range typical of γ Dor pulsators. A line-profile analysis inferred the presence of several high-degree modes, in the same low frequency range. Line-profile variations were confirmed by Mathias et al. (2004). In Fig. 1, we show the position of HD 49434 in a colour−magnitude diagram, based on the M_v value derived from the HIPPARCOS satellite and $(b-y)_0$, calculated from the photometric indices taken from Hauck & Mermilliod (1998) using the TempLogg method (Kupka & Bruntt 2001). We used the evolutionary tracks, instability strips, and ZAMS described by Poretti et al. (2003). As can be seen, HD 49434 is located close to the blue border of the γ Dor instability strip, and inside the instability strip of δ Sct stars.

2. Observations

2.1. Multi-colour photometry

Strömgren observations were completed with the twin Danish six-channel *uvbyβ* photometers at Sierra Nevada Observatory (SNO), Spain, and at San Pedro Mártir Observatory (SPMO), Mexico. The instruments were mounted on the 90-cm and 1.5-m telescopes, respectively. The data were collected using the four *uvby* filters and exposure times were 30 s. We used HD 48922 (V = 6.77 mag, A0) as a comparison star and HD 43913 (V = 7.88 mag, A0) as a check star.

Table 2. Logbook of the spectroscopic observations of HD 49434.

Instrument	#	# Nights (d)	ΔT (d)	S/N	S/N-range	$T_{\rm exp}$ (s)	Resolution	Range (Å)	Spectral gaps
FOCES	47	1	0.3	185	[110, 230]	300	40 000	3500–10 280	yes
FEROS	71	14	26.1	240	[100, 320]	120, 180	48 000	3500–9200	no
SOPHIE	377	14	20.2	165	[80, 240]	600, 500, 450	70 000	3870–6940	no
HERCULES	194	9	16.1	172	[110, 230]	600, 480, 420	35 000	4500–7300	yes

In total, we obtained 1353 data points of HD 49434 in 62 clear nights at SNO (January 2005; December 2005; January–March 2006; November 2006; January–March 2007; November–December 2007; January 2008) and 614 data points in 29 clear nights at SPMO (November 2005; November–December 2006; November–December 2007). We note that an important step in the reduction process was the correction for the instantaneous extinction coefficient, to suppress artificial/spurious frequencies in the 0–5 d^{-1} range (Poretti & Zerbi 1993). The standard deviations of the magnitude differences between the comparison and check stars (both measured in the same observational cycle) provide an indication of the precision of the data. We obtained values close to 12.3 mmag and 6.5 mmag (u light), 3.0 mmag and 4.2 mmag (v light), 3.0 mmag and 3.8 mmag (b light), and 3.0 mmag and 4.7 mmag (y light) for SPMO and SNO, respectively. The large scatter in data acquired in the u-light at SPMO is due to some instrumental problems with the photo-multiplier of the u channel.

Johnson *UBVRI* measurements were obtained with a single channel Peltier-cooled photo-electric photometer on the 50-cm Cassegrain telescope at the Piszkéstetõ Mountain Station of Konkoly Observatory (KO) from March 21 to 25, 2003. The comparison star used was again HD 48922, as well as HD 49933 ($V = 5.78$ mag, F2V). The latter comparison star, a solar-like oscillator, was also a CoRoT target. Exposure times for individual data points were 15 s. Consecutive three data points were added together to create 31 measurements with 45 s integration time each.

A logbook of the photometric observations obtained between March 2003 and March 2007 at SNO, SPMO, and KO is given in Table 1, which is only available in the online version of the paper. In Table 1, the observing date corresponds to the UT at the beginning of the observation and Julian Dates are given with respect to $JD_0 = 2\,450\,000$. An example of the light curve is given in Fig. 2. The differential light curves of HD 49434 show a complicated variable behaviour with variations on different timescales.

We also included data acquired by the HIPPARCOS satellite (Perryman et al. 1997) in our photometric analysis.

2.2. High-resolution spectroscopy

The spectroscopic observations were completed between December 2006 and February 2007 with FEROS@2.2-m ESO/MPI telescope, La Silla, Chile, with SOPHIE@1.93-m telescope at Observatoire de Haute Provence (OHP), France, with FOCES@2.2-m at Calar Alto Astronomical Observatory (CAHA), Spain, and with HERCULES@1.0-m McLellen Telescope at Mount John University Observatory (MJUO), New Zealand. A general logbook of the spectroscopic data of HD 49434 is given in Table 2. For each instrument we report the number of high-quality spectra, i.e. spectra that satisfy signal-to-noise ratio (S/N) > 80 in the regions near 4900 Å and 5700 Å, the number of successful nights, the time-span expressed in days, the average S/N, the range of S/N, the typical exposure times expressed in seconds, the resolution of the spectrograph, and the spectral range of the spectra. The last column of Table 2 indicates if there are gaps in the spectral coverage (yes/no). A log file of the individual observing nights, only available in the online version of the paper, is presented in Table 3. In this table, the observing date corresponds to the UT at the beginning of the observation, and Julian Dates are given with respect to $JD_0 = 2\,450\,000$. The time distribution of the spectroscopic observations can be seen from Fig. 7. The time-span with respect to the photometric observations is indicated by a black full line in Fig. 2.

2.2.1. The SOPHIE instrument

The new SOPHIE spectrograph, mounted on the 1.93-m telescope at OHP, is the successor of ELODIE. One of its main properties is its stability in performing asteroseismic observations. The SOPHIE spectrum, recorded on 39 non-overlapping spectral orders, ranges from 3870 to 6940 Å. The spectra were extracted and automatically reduced in real-time using a data reduction software package directly adapted from HARPS. Only the normalisation process was completed manually, after a correction to the heliocentric frame, by fitting typically a cubic spline.

Observations were completed during January 11–20 and January 27–February 1, 2007, representing 14 nights. Only 1.5 nights were lost due to adverse meteorological conditions. The 410 SOPHIE spectra of HD 49434 were obtained in the High-Resolution mode ($R \sim 70\,000$), since we focus on the study of line-profile variations (LPV).

2.2.2. FEROS data

The Fiber-fed, Extended Range, Échelle Optical Spectrograph (FEROS), mounted on the 2.2-m ESO/MPI telescope at La Silla (ESO), has a spectral resolution of $R \sim 48\,000$ and records spectra for almost the complete range of 3500–9200 Å on 39 échelle orders. The detector is a EEV 2k × 4k CCD. For the observations of HD 49434, we used the following set-up: the object+sky fiber combination, 1 × 1 binning mode, and the Atmospheric Dispersion Corrector enabled. We reduced the spectra using an improved version of the standard FEROS pipeline, written in MIDAS, developed by Rainer (2003). The main improvements in this pipeline concern the blaze and flat-field correction of the spectra, by using an accurate definition of the blaze function extracted from a well-exposed spectrum of a hot star. The reduced spectra were subsequently corrected to the heliocentric frame. We used an automated continuum normalisation procedure developed by Bossi (INAF OAB-Merate) to normalise the spectra with continuum at unity. Since the normalised spectra have to be treated with caution when performing a study of individual

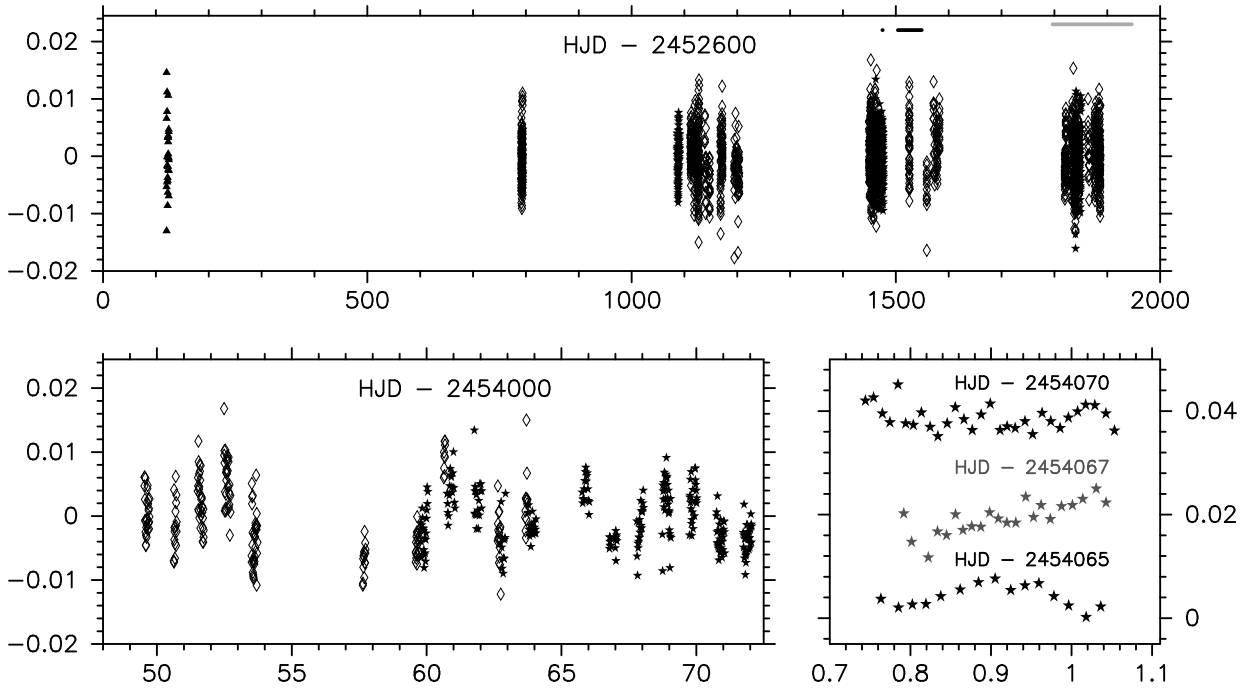

Fig. 2. Ground-based light curves of HD 49434. *The top panel* shows all relative KON Johnson V (triangles), SNO Strömgren y (open diamonds) and SPMO Strömgren y (stars) magnitudes. *The bottom left panel* zooms in on SNO and SPMO data obtained in November 2006. *The bottom right panel* shows the light curves obtained during the nights of 26 and 28 November 2006, and 1 December 2006 at SPMO. We plotted the individual nights with an offset of 2.1 mmag for clarity. On *top of the figure* we indicated the time span of the spectroscopic ground-based observations described in this paper (see Sect. 2.2) with a black line, while the continuous CoRoT observations are given in gray.

line-profiles, selected spectral regions (e.g. close to Ti II 4501.273 Å and Fe II 4508.288 Å) were also normalised manually by fitting cubic splines.

HD 49434 was one of the selected CoRoT targets observed during the 15 nights of January 1–10 and January 24–28, 2007, awarded in the framework of an ESO Large Programme (LP178.D-0361; PI: Poretti). We were able to observe for 85% of the total available time in good weather conditions, which enabled us to acquire 73 spectra.

2.2.3. HERCULES data

The High Efficiency and Resolution Canterbury University Large Echelle Spectrograph (HERCULES) is fibre-fed from the 1.0-m McLellan telescope at MJUO. The instrument has a resolution of $R \sim 35\,000$ and records selected regions of the spectral range of 3800–8800 Å in 48 orders. A description of the gaps in the spectral coverage was given by Hearnshaw et al. (2002). Unfortunately, the Ti II and Fe II profiles close to 4500 Å belong to one of those gaps. The spectra were reduced with a semi-automated procedure using the HERCULES Reduction Software Package version 2.3 (Skuljan 2004). After a correction to the heliocentric frame, the spectra were normalised using the automated continuum normalisation procedure described in Sect. 2.2.2.

Observing time was awarded on HERCULES during February 1–18, 2007, but half of these nights were lost due to bad weather. In total, 194 spectra were acquired. Exposure times ranged from 8 to 10 min in clear sky conditions, to 20 min when observing through thin clouds.

2.2.4. FOCES data

The FOCES échelle spectrograph on the 2.2-m telescope at CAHA has a spectral coverage of 3820–10 280 Å in 93 spectral orders. The recorded spectral range shows gaps for wavelengths redder then 8450 Å. The CCD is a Loral 2k × 2k CCD with a pixel size of 15 μm. For the observations of the γ Dor target, we used the $R \sim 40\,000$ mode. Since no pipeline is available, the spectral reduction and subsequent heliocentric correction were performed using standard IRAF échelle spectral reduction procedures. The spectra were normalised using an automated continuum normalisation procedure.

A total of 25 nights were awarded on FOCES to observe HD 49434. The time was distributed over two campaigns in December 2006 and 2007, with 5 more nights in February 2008. Unfortunately, bad weather hampered these runs reducing the usable data to only one night. A total of 47 FOCES spectra of HD 49434 were observed on December 4, 2006.

3. Analysis

3.1. Multi-colour analysis

The Strömgren dataset consists of 4 seasons of SNO observations and 3 seasons of SPMO data, of which the most continuous dataset (361 datapoints in 18 nights) was observed at SPMO in November–December 2006 (see also Fig. 2). We first searched for frequencies in data for all filters of the individual seasons, using SCARGLE (Scargle 1982) and Phase Dispersion Minimisation (PDM, Stellingwerf 1978) analysis, and the least-squares power spectrum method (Vaníček 1971). The runs in 2005 at SNO and SPMO were too short, with a time span of 2 and 4 days, respectively, to resolve the γ Dor type

periods. For other seasons, apart from the SNO subset obtained in November 2007–January 2008, we detected a frequency close to 0.24 d^{-1}, which is present in all filters. In the SNO datasets, a frequency of 1.73 d^{-1} was also detected.

Since individual seasons have different zero points due to instrumental effects, we aligned the data before merging them. The alignment was performed in a delicate and iterative process. We calculated the preliminary frequency solution of the individual subsets (i.e. we performed a least-squares fit with the frequency 0.24 d^{-1}), and used the constant of the fit to re-align the subsets at the same mean brightness level. Then, we determined an improved frequency solution from the merged dataset, and calculated, from the individual subsets, the least-squares fit with this new solution to obtain an improved value of the constant, which was then used to construct an improved merged dataset. We continued this iterative process until an optimized multi-periodic solution was found (see below). The value of the constant of the least-squares fit at the end of the iterative process did not differ by more than 0.2 mmag from the constant calculated in the first iteration step, for all filters. We are aware that this artificial alignment can remove or modify long-period variations, if present. To quantify the artificial shifts, we provide a list, for each filter, of the relative correction between the subsets of the SPMO data and SNO data separately, as well as the relative offset between the SPMO and SNO datasets. The relative corrections between the SPMO subsets are of the order of 18.1 mmag (u filter), 21.9 mmag (v filter), 24.7 mmag (b filter), and 6.8 mmag (y filter). For the SNO subsets, the corrections are 20.3 mmag (u filter), 9.7 mmag (v filter), 6.3 mmag (b filter), and 6.7 mmag (y filter). The offset between the SPMO and SNO subsets are of the order of 20.0 mmag (u filter), 21.0 mmag (v filter), 41.0 mmag (b filter), and 9.0 mmag (y filter).

In the aligned datasets, a frequency close to 1.7348 d^{-1} appears as well as 0.2342 d^{-1}, and, has the highest amplitude. More low-amplitude frequencies appear to be present in the light variations (such as 2.538 d^{-1} and 2.253 d^{-1}), but without further evidence we only accept the two frequencies that satisfy the $S/N > 4$ criterion (Breger et al. 1993; Kuschnig et al. 1997): 1.73480(3) d^{-1} and 0.23427(5) d^{-1}. The S/N level was computed as the average amplitude over a frequency interval of width 5 d^{-1} in an oversampled SCARGLE periodogram obtained after final prewhitening. We carefully checked if the two frequencies were independent (their sum was close to, but significantly different from, 2 d^{-1}), and found convincing evidence that they independently contribute to the variability: at different stages of the prewhitening procedure, both frequencies are detected. The same results were also obtained when applying the Vaníček method (Vaníček 1971), which does not rely on the concept of prewhitening, since the amplitudes and phases of the known terms are recalculated for each new trial frequency. The frequency errors listed in Table 4 are calculated using the formula described by Montgomery & O'Donoghue (1999).

We also derived merged datasets (V light) consisting of Strömgren y data (SPMO and SNO), Johnson V data (KON), and/or HIPPARCOS data. To add the KON and/or HIPPARCOS data, we used the same alignment procedure as described above. We note that the individual KON Johnson dataset was too short in duration to detect accurate frequencies. Unfortunately, by analyzing the HIPPARCOS dataset only (ΔT = 1095 d; 104 datapoints), we were unable to detect any frequency. The frequency search was hampered by a combination of a bad observing window (the highest frequency in the observing window was 0.2311 d^{-1}, which is exactly of the order of the γ Dor-type frequencies that we are looking for) and the low-amplitudes

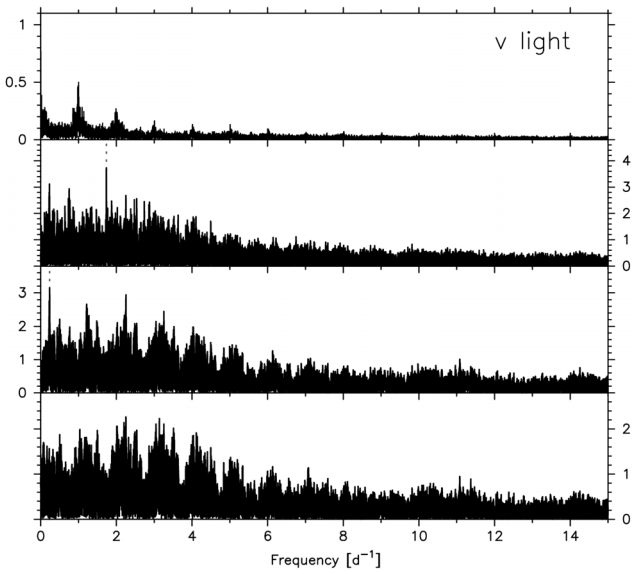

Fig. 3. SCARGLE periodograms calculated from the Strömgren v data (SPMO and SNO) of HD 49434. *The top panel* indicates the associated spectral window, followed by the periodogram of the observed light variations, and those calculated after subsequent removal of the frequencies 1.73480 d^{-1} and 0.23427 d^{-1}. These two frequencies are indicated by dashed gray lines. The amplitudes are expressed in mmag.

of the intrinsic frequencies of HD 49434, which were hidden in the noise. In the merged V light datasets, we did not measure frequencies other than those detected in the Strömgren datasets alone. Given the inconvenient time sampling of the HIPPARCOS data and the short duration of the KON data, we decided to be conservative and, despite its longer time-span, to keep the frequency accuracy derived from the Strömgren dataset. The SCARGLE periodograms of the Strömgren v light are shown in Fig. 3. The solution of the least-squares fit of the bi-periodic model with 1.73480 d^{-1} and 0.23427 d^{-1} calculated from the *uvby* time-series of HD 49434 is given in Table 4. Errors in units of the last digit are given in parentheses. For each filter the total variance reduction of the bi-periodic model and the root mean square (rms) of the residuals is reported. Phase = 0 corresponds to T_0 = 2 454 057.2640.

It is striking to discover that we are unable to explain the major part of the observed light intensity variations of HD 49434 in our ground-based photometric dataset. Several other low-amplitude oscillations probably also contribute to the light variability. From the nightly variations (see bottom right panel in Fig. 2), we suspect the presence of periods of the order of a few hours as well. As can be seen in the bottom panel of Fig. 3, the power excess at this spectral region is low. To provide a quantitative comparison, we computed the mean level of the noise in the residual dataset for three separate regions: 0–5 d^{-1}, 5–10 d^{-1}, and 10–15 d^{-1}. We obtained a mean noise level of 0.45 mmag, 0.25 mmag and 0.22 mmag, respectively. We refer to Sect. 3.3 for a further discussion of the subject.

3.2. Spectroscopic analysis

In addition to individual line profiles, such as those of Ti II 4501.273 Å and Fe II 4508.288 Å (right panel Fig. 4), we considered deconvoluted profiles computed by the Least-Squares Deconvolution (LSD) method (Donati et al. 1997, 1999). The LSD method extracts an average line profile from

Table 4. Solution (amplitudes and phases) of the least-squares fit of the bi-periodic model with 1.73480 d^{-1} and 0.23427 d^{-1} calculated from the *uvby* time-series of HD 49434.

Freq. (d^{-1})	Strömgren *u*		Strömgren *v*		Strömgren *b*		Strömgren *y*	
	Ampl (mmag)	phase (rad)	Ampl (mmag)	phase (rad)	Ampl (mmag)	phase (rad)	Ampl (mmag)	phase (rad)
1.73480	2.5(3)	5.8(1)	3.4(2)	5.84(5)	3.1(2)	5.86(5)	2.4(1)	5.89(6)
0.23427	1.8(3)	3.5(2)	2.5(2)	3.80(7)	2.1(2)	3.80(8)	1.6(1)	3.80(8)
Var. Red.	5.9%		24.7%		24.4%		21.2%	
Residual rms (mmag)	9.0		6.0		6.0		5.0	

Phase = 0 corresponds to T_0 = 2454057.2640.

several hundreds of individual lines by comparing them with synthetic line masks. We used the spectral line list from the VALD database (Piskunov et al. 1995; Ryabchikova et al. 1999; Kupka et al. 1999). We chose a mask with $T_{\rm eff}$ = 7250 K and $\log g$ = 4.0 and included all elements apart from He and H. We calculated the LSD profiles from the regions 4380–4814 Å and 4960–5550 Å, which involved combining the information of more than 3100 lines of FEROS, SOPHIE and FOCES spectra, and 1700 lines of HERCULES spectra. Using this method, we increased the relatively low S/N of the spectra by creating for each spectrum a single profile with an average S/N of 5000, 2800, 1900 and 1400 for the FEROS, SOPHIE, HERCULES, and FOCES spectra, respectively. Since the average line profiles did not have a continuum level at 1.0, the LSD profiles were subsequently normalised. The LSD profiles calculated from different instruments were found to have different depths, while the depth of the LSD profiles from the same instrument were comparable. To homogenize the profiles derived from observations with different instruments, a scale-factor was computed from the average LSD profile per dataset, and applied to rescale all profiles to comparable line depths. We note that the absolute RV values calculated from the LSD profiles do not have physical meaning, but the relative RV changes are intrinsic to the star. A selection of the final LSD profiles are presented in Fig. 4. The RV steps of the individual LSD profiles were 1 km s^{-1} (SOPHIE), 2 km s^{-1} (FEROS and FOCES) and 2.5 km s^{-1} (HERCULES). We did not find evidence that HD 49434 had a binary nature in the line profiles. We discovered the existence of systematic instrumental differences in the FEROS, SOPHIE, HERCULES, and FOCES spectra. For instance, the FOCES spectra appeared to be blue shifted by ~1.5 km s^{-1} with respect to the profiles obtained with the FEROS and SOPHIE instruments, while the HERCULES spectra were shifted slightly towards the red. To correct for instrumental effects, we shifted the spectra from each dataset by a fixed RV value ("aligned profiles"). The values were determined to be the average of the first normalised moment, and were −12.8327 km s^{-1}, −13.3156 km s^{-1}, −13.7354 km s^{-1}, and −15.1830 km s^{-1}, for HERCULES, SOPHIE, FEROS and FOCES spectra, respectively.

We computed the first zero-point position of the Fourier transform for the mean LSD profile of each instrument, which provides an indication of the $v \sin i$ for a star (Gray 2005), assuming that rotation is the primary contributor to the line broadening. We derived the same value $v \sin i = 87 \pm 1$ km s^{-1} from all FEROS, SOPHIE, HERCULES and FOCES spectra, to within error margins.

We searched for intrinsic frequencies by applying two line-diagnostics: the pixel-to-pixel variations across the line profile and the moment variations.

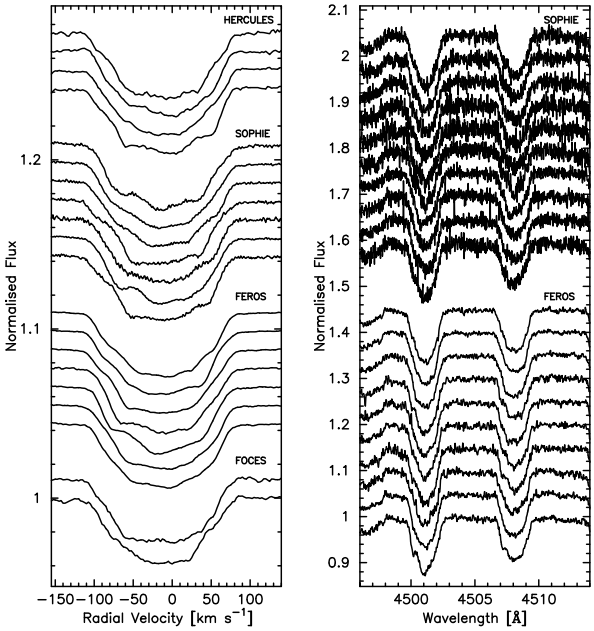

Fig. 4. *Left*: a selection of LSD profiles calculated from the HERCULES, SOPHIE, FEROS and FOCES spectra of HD 49434. *Right*: a selection of SOPHIE and FEROS spectra of HD 49434, centred on the Ti II 4501.273 Å and Fe II 4508.288 Å profiles. The spectra are offset for clarity.

3.2.1. Variations across the line profile

To detect variable signals in the time series of each pixel of the profile, we used the two-dimensional Fourier transform analysis method (Intensity Period Search (IPS) Method, Telting & Schrijvers 1997). To optimise the frequencies and remove false peaks from the power spectra, we applied the CLEANEST algorithm (Foster 1995) at the positions of the first and second zeros of the Fourier transform for the individual profiles.

Figure 5 presents the two-dimensional dynamic spectra evolution of the FEROS, SOPHIE and HERCULES LSD profiles. Travelling bumps are easily observed moving from blue to red. A pattern of high frequencies dominates the LPV. Variations in the blue wing have clearly higher amplitudes than those in the red wing. This fact has already been reported for individual line profiles (Mathias et al. 2004): it is probably caused by equivalent width (EW) variations in the intrinsic profile, which find their origin in local temperature variations on the stellar surface, due to pulsations (Schrijvers & Telting 1999). Schrijvers & Telting (1999) showed that non-adiabatic modes can cause a non-adiabatic phase-lag in the temperature (or EW) response, which is observed as an asymmetry in the IPS (see also Fig. 9).

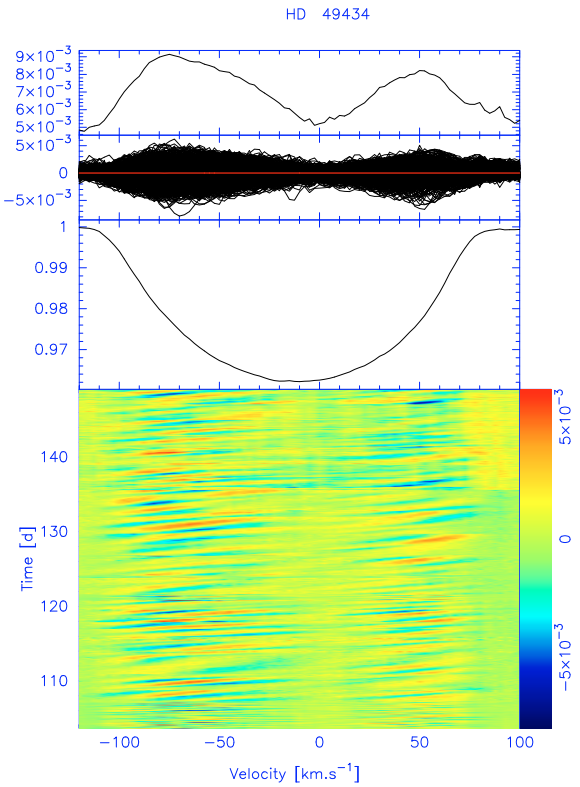

Fig. 5. *Lower part*: Bi-dimensional plot of the temporal evolution (on an arbitrary scale) of the residual FEROS, SOPHIE and HERCULES LSD profiles of the star HD 49434. *Upper part*: *from bottom to top* are successively represented the mean spectrum, the individual residual spectra and the dispersion σ around the mean residual.

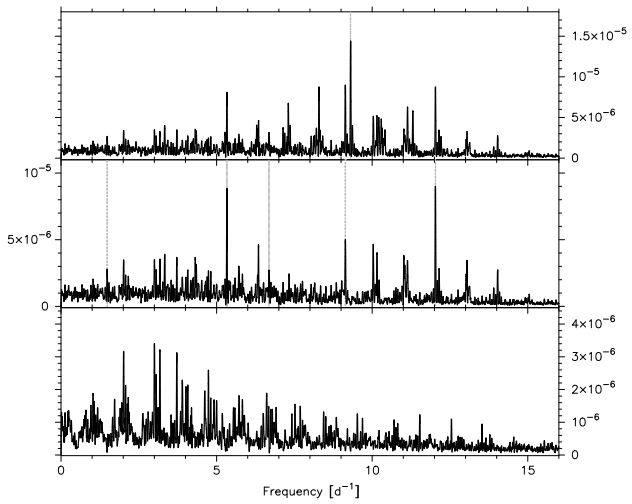

Fig. 6. Summed power over each pixel of the LSD profiles of the Fourier power spectra calculated from the combined dataset of FEROS, SOPHIE and HERCULES LSD spectra, which is a measure for the amplitude of the variability. *The top panel* gives the power spectra calculated from the original profiles. *The middle panel* shows the power spectra after removal of the dominant frequency (9.302 d^{-1}). At *the bottom* the residual power spectra are shown after prewhitening the six frequencies 9.3070 d^{-1}, 5.3311 d^{-1}, 12.0332 d^{-1}, 9.1527 d^{-1}, 6.6841 d^{-1} and 1.483 d^{-1}, which are indicated by the light grey dotted lines.

We analysed all individual datasets and the combined sets. Unfortunately, combining the datasets reduced the RV resolution because we had to rebin the profiles to identical RV step per pixel. The total time span of the joined FEROS, SOPHIE and HERCULES spectra (648 spectra) measures 45.4 days. By co-adding the 47 FOCES spectra, we obtained a time base of 75 days.

Our search for frequencies in the pixel-to-pixel variations of the LSD line profile data, in the range −105 to 101 km s^{-1}, discovered at least six frequencies (see Table 6). We accepted only frequencies that were clearly present in the individual datasets, as well as frequencies for which we found additional evidence in the moment variations (see Sect. 3.2.2). The dominant frequency was 9.3070(3) d^{-1}, followed by 5.3311(3) d^{-1}, 12.0332(3) (or 11.0332) d^{-1}, 10.1527(7) (or 9.1527) d^{-1}, 6.6841(7) (or 7.6841) and 1.4831(8) d^{-1}. For three of the frequencies we were unable to differentiate between the frequency and one of its one-day aliases. The errors in the frequencies, as calculated from Montgomery & O'Donoghue (1999), are given in parentheses. The residual signal after removing the six frequencies revealed the presence of other periodicities, but given the low-amplitudes and the fact that we were unable to differentiate between a frequency and several of its aliases we adopted a conservative attitude. Candidate frequencies that we did not accept without additional evidence are 3.182 d^{-1} and 3.720 d^{-1}, or one of their aliases.

The averaged Fourier power spectrum for the combined dataset of FEROS, SOPHIE, and HERCULES LSD profiles is given in Fig. 6. The bottom two panels show the Fourier spectra after prewhitening with the dominant first frequency (9.3070 d^{-1}) and the residuals after prewhitening with the six frequencies described above, which are indicated by dashed gray lines.

Similar frequencies were measured by the pixel-to-pixel analysis of the individual Ti II 4501.273 Å and Fe II 4508.288 Å profiles.

3.2.2. Moment variations

A moment analysis was performed by considering the EW and the first three normalised moments ($\langle v\rangle, \langle v^2\rangle, \langle v^3\rangle$, e.g. Aerts et al. 1992), calculated from the Ti II 4501.273 Å, Fe II 4508.288 Å, and LSD line profiles, using fixed integration boundaries of [4498.30, 4503.40] Å, [4505.40, 4510.70] Å, and [−94.4, 91.0] km s^{-1}, respectively. We analysed the corresponding time-series using the least-squares power spectrum method and SCARGLE and PDM analyses. Figure 7 shows the first normalised moments calculated from the LSD profiles (upper panel) and the Ti II and Fe II profiles (bottom panel). It is clear that due to the low S/N of the individual spectra, the different instrumental properties, the strong dependence of the moment measurements on the S/N value and the normalisation accuracy, the scatter in the calculated moments from the Ti II and Fe II profiles is high, and differs for individual instruments (FEROS and SOPHIE measurements are represented by stars and bullets, respectively). A moment analysis of the individual profiles did not provide satisfactory results. We therefore describe only the results obtained from the far more accurate LSD profiles.

We again considered both the individual and the combined data sets. We were unable to detect a clear periodicity in the EW variations. The individual FEROS, HERCULES, and FOCES moments are affected by noise with no dominant signal. We present an overview of the frequencies found in the moments of the combined FEROS, SOPHIE, and HERCULES data, which is illustrated in Tables 5, 6, and Fig. 8. The addition of one night of lower quality FOCES data did not improve the

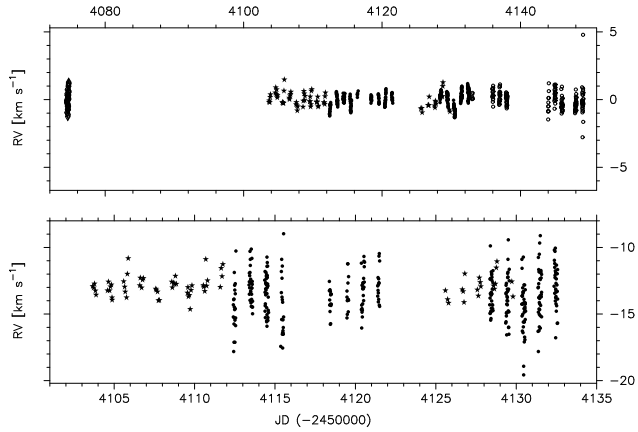

Fig. 7. First normalised moments (RVs) calculated from the FEROS (stars), SOPHIE (bullets), HERCULES (open circles) and FOCES (triangles) spectra of HD 49434. *Top panel*: $\langle v \rangle$ calculated from the LSD profiles after correction for the small velocity shifts between different datasets resulting from systematical instrumental differences. *Bottom panel*: average value of $\langle v \rangle$ calculated from the Ti II and Fe II profiles near 4500 Å of the FEROS and SOPHIE spectra. We used the same relative scale in y-axis in *top and bottom panel* to illustrate the scatter difference between the RVs measured from the LSD profiles and from the individual profiles.

Table 5. Amplitudes of the contribution of the frequencies to the variability in the first three moments calculated from the LSD profiles of the combined FEROS, SOPHIE and HERCULES spectra of HD 49434.

Frequency (d^{-1})	$\langle v \rangle$ Ampl ± s.e. ($km\,s^{-1}$)	$\langle v^2 \rangle$ Ampl ± s.e. ($(km\,s^{-1})^2$)	$\langle v^3 \rangle$ Ampl ± s.e. ($(km\,s^{-1})^3$)
0.234	0.22 ± 0.03	5 ± 1	651 ± 189
1.2732	0.32 ± 0.03	16 ± 1	2374 ± 188
1.489	0.20 ± 0.03	12 ± 1	1055 ± 189
5.583	0.14 ± 0.03	12 ± 1	433 ± 185
9.308	0.09 ± 0.02	3 ± 1	1076 ± 180
2.666	0.17 ± 0.03	3 ± 1	954 ± 190
frac. var.	36.8%	30.0%	28.4%

Table 6. Overview of the detected frequencies in the variability of HD 49434.

Freq (d^{-1})	$\langle v \rangle$	$\langle v^2 \rangle$	$\langle v^3 \rangle$	LPV	Photometry
0.23427(5)	x	...	...	...	x
1.2732(8)	x	x	x	...	...
1.4831(8)	x	x	...	x	...
1.73480(3)	...	...	...	...	x
2.666(2)	x	...	...	...	...
5.3311(3)	...	...	...	x	...
5.583(1)	x	x	...	...	...
9.3070(3)	...	...	x	x	...
6.6841/7.6841	...	...	...	x	...
10.1527/9.1527	...	...	...	x	...
12.0332/11.0332	...	...	...	x	...

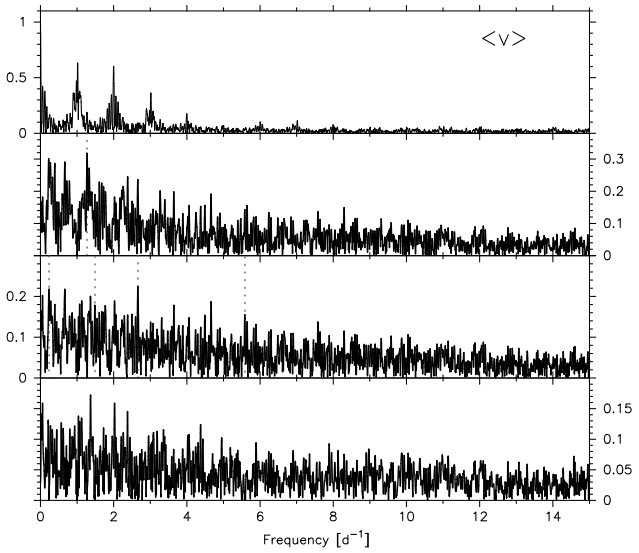

Fig. 8. SCARGLE periodograms calculated from the first moment of the combined FEROS, SOPHIE, and HERCULES LSD profiles. *The top panel* indicates the associated spectral window. We then plot, *from top to bottom*: the periodogram of the first moment, the one after prewhitening with 1.2732 d^{-1}, and the one after additional removal of 2.666 d^{-1}, 0.234 d^{-1}, 1.489 d^{-1} and 5.583 d^{-1}. The listed frequencies are indicated by light grey lines. The amplitudes are expressed in $km\,s^{-1}$.

frequency solution but only added noise and was omitted from the analysis. We accepted frequencies that satisfied the $S/N > 4$ criterion, as well as low-amplitude frequencies for which we found evidence in more than one line-diagnostics and/or in the multi-colour variations.

The dominant frequency in all moments was 1.2732(8) d^{-1}. In the first moment, we additionally found 2.666(2) d^{-1}, 0.234(1) d^{-1}, 1.489(2) d^{-1} and 5.58(1) d^{-1}. The last two frequencies had low amplitudes, but we accept them because they were confirmed by variations in the second and higher order ($\langle v^4 \rangle, \langle v^5 \rangle, \langle v^6 \rangle$) moments and/or by the line-profile analysis. On the other hand, the frequency 2.666 d^{-1} was only detected by variations in the first moment, and not in any other diagnostics. However, the first harmonic of this frequency is fairly close to 5.3311 d^{-1}, which is found in the line-profile analysis. We note that the contribution of 5.3311 d^{-1} in the variations of the first moment was not significant. The frequency 0.234 d^{-1} was also detected in multi-colour variations (see Sect. 3.1). In the residuals of the first moment evidence for several other periodicities (e.g. 1.369 d^{-1} and 2.024 d^{-1}) is clear, but requires confirmation by a more extended and accurate dataset, such as CoRoT, before being accepted as real. Figure 8 shows the SCARGLE periodogram calculated from the first moment of the combined dataset.

Besides the dominant frequency 1.2732(8) d^{-1}, the second moment shows variations with 1.489(1) d^{-1} and 5.583(1) d^{-1}. The frequency 1.489 d^{-1} was also detected in the line-profile analysis (see Sect. 3.2.1). We accept only these three frequencies, even though the residual time-series appears to show other periodicities (e.g. 4.629 d^{-1}).

In the third moment, we detected only one additional frequency, 9.308(2) d^{-1}, which is the dominant frequency found in the pixel-to-pixel variations across the line-profile.

In summary, in the moment variations we found evidence for a total of five frequencies, of which two were already detected in the line-profile variations (see Sect. 3.2.1) and one was discovered in the photometric dataset (see Sect. 3.1). Additionally, we detected the frequency 2.666 d^{-1} in the variations of the first moment, which appears to be the double period of frequency 5.3311 d^{-1}. A possible explanation for the detection of both frequencies is a rotational effect caused by the presence of a

surface inhomogeneity, with rotational frequency $f_{\rm rot} = 2.666\ {\rm d}^{-1}$. Given a stellar radius of $R = 1.601\ R_\odot$ (Masana et al. 2006) and a $v \sin i$ value of 87 km s^{-1} (see Sect. 3.2), we found the lower limit $f_{\rm rot} > 1.07\ {\rm d}^{-1}$ for HD 49434. These values of R and $v \sin i$, assuming $f_{\rm rot} = 2.666\ {\rm d}^{-1}$, imply an inclination angle $i = 24°$, an equatorial velocity $v_{\rm eq} = 236$ km s^{-1}, and that HD 49434 is a fast rotator. Obviously, we need to investigate if $2.666\ {\rm d}^{-1}$ can indeed be identified as the rotational frequency.

The results of least-squares fitting of the data with models of six frequencies is given in Table 5. The total variance of reduction is given at the bottom of the table. The best-fitting model accounts for 37%, 30% and 28% of the total observed variability in the first, second, and third moment, respectively. We expect that HD 49434 oscillates in other additional modes with amplitudes below our current detection limit. Continuous and accurate CoRoT light curves promise invaluable additional information to unravel the frequency spectrum of HD 49434.

3.3. Frequency summary

Table 6 provides an overview of all detected frequencies with an indication (x) of the diagnostic (moments, line profiles, or light variations) for which the variation is predominantly present. The errors on the frequencies, as calculated from Montgomery & O'Donoghue (1999), are given between brackets. In total, we detected nine bona fide frequencies, of which three show an ambiguity concerning their value. The frequency 2.666(2) d^{-1} can possibly be interpreted as the rotational frequency $f_{\rm rot}$ of the star. The frequency 5.3311 d^{-1} might be the first harmonic of the rotational frequency, and point towards the presence of surface inhomogeneities, although this hypothesis needs confirmation. We propose other candidate frequencies 3.182 d^{-1} and 3.720 d^{-1} or one of their aliases, for which we need additional evidence. We did not find obvious relations (combination effects or aliases) between the proposed frequencies. In particular, the frequencies at 1.27 d^{-1} and 1.73 d^{-1} (their sum gives 3 d^{-1}) appear to be independent, since the photometric (spectroscopic) data can not be fitted well by the 1.27 d^{-1} (1.73 d^{-1}) term.

We detected excess power in two separate regions of the frequency spectrum: one centred on 1.5 d^{-1} and one at higher frequencies, between 5 and 12 d^{-1}. The first region is characteristic of γ Dor pulsators and the second range is typical of δ Sct stars. The presence of both p- and g-types pulsation is not unexpected, given the location of the star close to the hot border of the γ Dor instability strip and within that of δ Sct pulsators (see Fig. 1). We propose that HD 49434 is a new hybrid γ Dor/δ Sct variable. In the multi-colour variations we detected only γ Dor type of variations at significantly high amplitudes. We could barely detect traces of the spectroscopic frequencies in the photometric data (amplitudes <0.6 mmag), probably because the high-degree modes (see Sect. 4) cannot be detected in the integrated light. It is puzzling that the dominating frequency of the moments 1.2732 d^{-1} is not detected in the pixel-to-pixel variations. As our frequency model can only explain a small portion of the total observed variability, which is a common problem in γ Dor star studies (Mathias et al. 2004), we expect that other pulsation frequencies are present, but could not be detected due to the limitations of our ground-based dataset, such as non-continuous time sampling and a restricted amplitude accuracy. The exploitation of the continuous CoRoT space data of HD 49434 promises a break through in the understanding of this puzzling, challenging, and interesting target.

4. Mode-identification

4.1. Moment method

We attempted an identification of the dominant frequency in the velocity moments, 1.2732 d^{-1}, using the Moment Method by Briquet & Aerts (2003). This method scans the discrete (ℓ, m) space and other continuous velocity parameters, such as the inclination angle between the rotation axis and the line of sight, and the intrinsic width of the line profile. It searches for the combination that provides the closest fit between the observed and theoretical oscillation amplitude of the first moment. The discriminant value Σ is an indicator of the goodness of fit: the lower is the value of Σ, the closer is the agreement between theoretical and observed moment values. The Moment Method identifies a single mode accurately if its amplitude is far larger than the other detected signals. The identification of several modes simultaneously is more challenging and requires an accurate description of the frequencies and the amplitudes. Since our target HD 49434 shows several low-amplitude frequencies, we focused only on the identification of the highest amplitude mode, which is also the only mode detected in all three moments. We calculated Σ by assuming a stellar mass and radius of $M = 1.55\ M_\odot$ and $R = 1.6\ R_\odot$, respectively, which corresponded to a ratio of horizontal to vertical pulsation amplitude $K = 17.403$ for 1.2732 d^{-1}. Since HD 49434 is a fairly rapid rotator ($v_{\rm eq} \geq 87$ km s^{-1}), we used the formalisms with and without taking into account rotational effects (see Townsend 1997). The corresponding Σ values did not favour a specific solution nor discriminate between the different (ℓ, m) combinations. The results exclude a zonal mode and indicate a $5 \leq \ell \leq 7$ mode, which is probably tesseral. We tried to improve the results by suppressing the contribution of the additional low-amplitude variations by averaging the moments in phase bins of 0.025 of the oscillation cycle. This approach has been successfully applied to other stars (e.g. κ Sco, Uytterhoeven et al. 2004), but unfortunately did not provide satisfactory results for HD 49434. We note that 1.2732 d^{-1} only accounts for 21% of the total variability in the first moment. Reducing the scatter in the mono-periodic fit, we calculated Σ for a perfect theoretical time series of the same amplitude and phase properties as observed, which provided identification results similar to those described above. We therefore conclude that 1.2732 d^{-1} is probably a $5 \leq \ell \leq 7$ tesseral mode.

4.2. Intensity period search method

The modes detected in the pixel-to-pixel variations of HD 49434 can be identified using information about their phase distribution and phase distribution of their first harmonic across the line profile (IPS Method, Telting & Schrijvers 1997). We find that all modes have a high degree ($3 \leq \ell \leq 8$). This follows from the relations between the quantum numbers ℓ and m, and phase differences with respect to the frequency and its first harmonic, $\Delta\Psi_f$ and $\Delta\Psi_{2f}$, given by $\ell \approx 0.10 + 1.09|\Delta\Psi_f|/\pi$ and $|m| \approx -1.33 + 0.54|\Delta\Psi_{2f}|/\pi$, as derived by Telting & Schrijvers (1997). The formal errors on ℓ and m are of the order of 1 and 2, respectively. For detailed results, we refer to Table 7. In this table the blue-to-red phase differences, together with estimates for ℓ and m, are reported. We note that we also attempted to identify the frequency 5.3311 d^{-1}, even though this frequency might be due to surface homogeneities in combination with rotational effects. Since this hypothesis requires confirmation, we explore an explanation in terms of a non-radial pulsation mode as well. Figure 9 shows the mean profile of the observed data

Table 7. Mode-identification results for HD 49434 from the IPS Method (top) and the Moment Method (bottom).

Frequency (d^{-1})	$\Delta\Psi_f$ (π rad)	$\Delta\Psi_{2f}$ (π rad)	$\ell \in$	$\lvert m\rvert \in$
1.4831	5.0	6.0	[4, 6]	[0, 4]
5.3311	7.0	6.5	[6, 8]	[0, 4]
9.3070	5.0	7.0	[4, 6]	[0, 4]
7.6841(6.6841)	3.5	7.5	[3, 5]	[0, 4]
10.1527(9.1527)	6.5	~6	[6, 8]	[0, 4]
12.0332(11.0332)	6.5	3.5	[6, 8]	[0, 2]
1.2732	...	...	[5, 7]	$0 < \lvert m\rvert \leq l$

(top), the phase distribution (middle), and amplitude distribution (bottom) across the line profile, for each of the six frequencies detected in the pixel-to-pixel variations across the line profiles, listed in Table 6. As can be seen in Fig. 9, the amplitudes of most modes are low. We note that the candidate frequencies 3.182 d^{-1} and 3.720 d^{-1} (or one of their aliases), which we did not accept without additional evidence, show well defined phase distributions, and can be associated with modes for which $\ell \in [2, 4]$ and $\ell \in [6, 8]$, respectively.

We postpone the identification of the two photometric modes by means of the amplitude and frequency ratio methods to a subsequent paper, since the theoretical description of the pulsational character of HD 49434 is complicated, due to its rapid rotation ($v_{\rm eq} \geq 87$ km s^{-1}).

5. Abundance analysis

We performed an abundance analysis of the averaged normalised FEROS spectrum, due to its relatively high mean S/N-value compared to the other data sets. The synthetic spectra that we used, were computed with the SYNTHE code (Kurucz 1993) ported under GNU Linux by Sbordone et al. (2005). All the atmospheric models were computed with the line-blanketed LTE ATLAS9 code, which handles line opacity with the opacity distribution function method (ODF). We adopted the atomic line list from the VALD database (*Vienna Atomic Line Database*, Kupka et al. 1999; Ryabchikova et al. 1999).

For the analysis of the data an efficient spectral synthesis method based on the least-squares optimalisation algorithm was used (Takeda 1995; Bevington 1969). This method allows the simultaneous determination of various parameters involved with stellar spectra and consists of the minimisation of the deviation between the theoretical flux distribution and the observed one. The synthetic spectrum depends on stellar parameters such as effective temperature $T_{\rm eff}$, surface gravity $\log g$, microturbulence ξ, rotational velocity $v \sin i$, radial velocity, and relative abundances of the elements ϵ_i, where i denotes the individual element. The first three parameters were not determined during the iteration process but were considered as input values. All the other above mentioned parameters can be determined simultaneously because they produced detectable and different spectral signatures. The theoretical spectrum was fitted to the averaged normalised FEROS spectrum. All spectra were normalised using MIDAS procedures. In some parts of the blue wavelength range, the continuum level was corrected by comparison between theoretical and observed spectra.

We fixed the input $T_{\rm eff}$ and $\log g$ values to 7300 K and 4.2 dex, respectively (see Sect. 1). The abundances and rotational velocity provided by our analysis are presented in Table 8. Standard deviations are reported only if more than two spectral parts were used to determine the element abundance. In the last two columns of Table 8 the standard solar composition of Grevesse & Sauval (1998; Sun 1D) and solar abundances derived from 3D hydrodynamical models (Asplund et al. 2005; Sun 3D) are given. In all calculations, we assumed a microturbulence velocity ξ equal to 2 km s^{-1} (Bruntt et al. 2002). The obtained abundances are compared with previous results in Fig. 10. As we can see, the determined chemical composition of HD 49434 is close to the solar value. We derived a metallicity of $Z = 0.019 \pm 0.002$ for HD 49434, assuming solar values from Grevesse & Sauval (1998) for all elements not considered in our work. The most important discrepancy was found for Ba, but for this element only three lines were considered. Our results are consistent with all values obtained in previous analyses. The influence of changes in $T_{\rm eff}$, $\log g$, and microturbulence (e.g. Bruntt et al. 2002) on the derived abundances are shown in Table 9, available in the online version of the paper. Standard deviations are given only if more than two spectral parts were used to determine the element abundance. We derived the abundances of elements for $T_{\rm eff} = 7300 \pm 400$ K, $\log g = 4.2 \pm 0.1$ dex, and $\xi = 2 \pm 1$ km s^{-1}. The influence of effective temperature on the abundance is more important, especially for Mg, V and La, for which the difference is equal to about 0.4 dex. For the other

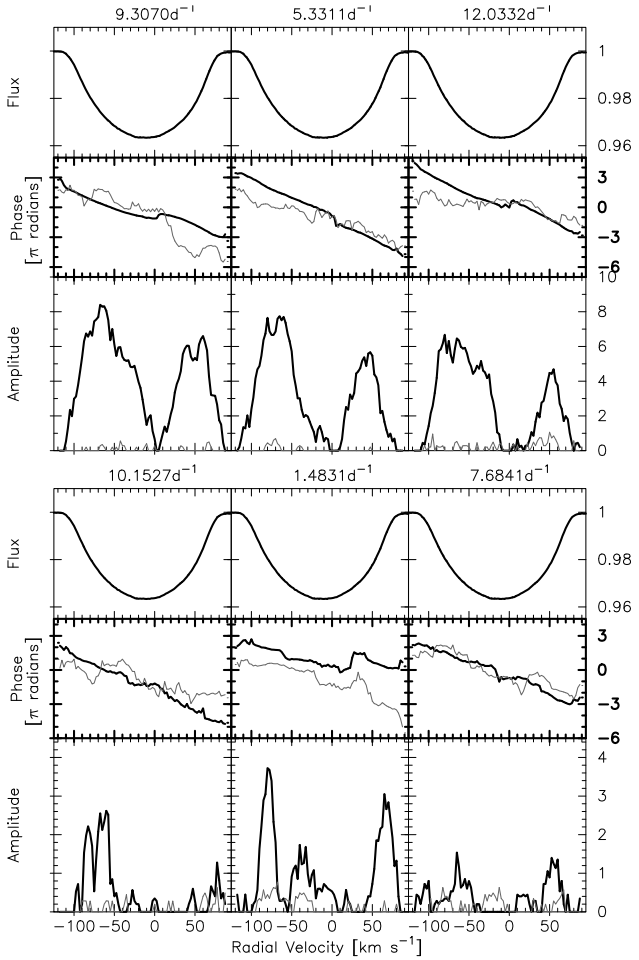

Fig. 9. IPS diagrams calculated from the FEROS, SOPHIE and HERCULES LSD profiles for the frequencies 1.4831 d^{-1}, 5.3311 d^{-1}, 9.3070 d^{-1}, 7.6841 (6.6841) d^{-1}, 10.1527 (9.1527) d^{-1}, and 12.0332 (11.0332) d^{-1}. *From top to bottom*: average line profile, phase and amplitude distribution across the line profile. Black and gray lines indicate phase and amplitude of a frequency and its harmonic, respectively.

Table 8. Average LTE abundances, $\log \epsilon(N)$, and standard deviations, σ ($\log \epsilon[\mathrm{H}] = 12$), of HD 49434 together with corresponding values of the standard solar composition.

N	$\log \epsilon(N)$	σ	Sun 1D	Sun 3D
C	8.70	0.14	8.52	8.39
O	8.86	...	8.83	8.66
Na	6.02	...	6.33	6.17
Mg	7.67	0.09	7.58	7.53
Si	7.52	0.47	7.55	7.51
S	7.31	...	7.33	7.14
Ca	6.60	0.16	6.36	6.31
Sc	3.52	0.28	3.17	3.05
Ti	5.10	0.22	5.02	4.90
V	4.25	0.30	4.00	4.00
Cr	5.87	0.23	5.67	5.64
Mn	5.37	0.35	5.39	5.39
Fe	7.50	0.12	7.50	7.45
Co	5.34	...	4.92	4.92
Ni	6.23	0.16	6.25	6.23
Cu	4.03	...	4.21	4.21
Y	2.51	0.18	2.24	2.21
Zr	2.74	0.15	2.60	2.59
Ba	3.24	0.06	2.13	2.17
La	1.17	...	1.17	1.13
Ce	2.13	...	1.58	1.58
Nd	1.18	...	1.50	1.45

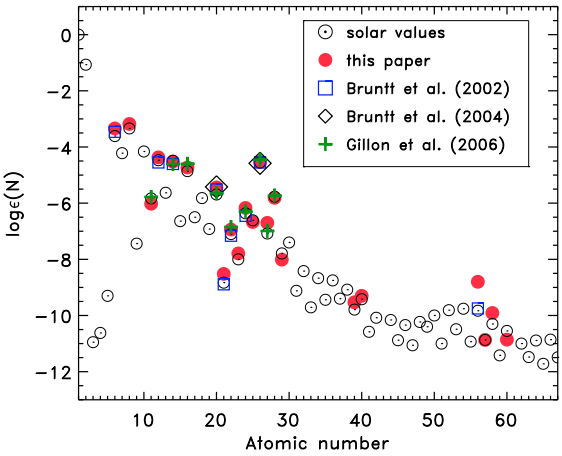

Fig. 10. Element abundances of HD 49434 derived in this paper (red bullets) compared to the solar values (Grevesse & Sauval 1998, ⊙), and the values obtained for HD 49434 by Bruntt et al. (2002, blue squares), Bruntt et al. (2004, black diamonds) and Gillon & Magain (2006, green crosses).

elements, changes in temperature produce variations in derived abundances of about 0.2 dex or lower.

6. Discussion and conclusion

We have presented frequency analysis and preliminary spectroscopic mode-identification results for HD 49434, obtained from the most extensive ground-based dataset for a γ Dor star to date. Photometric and spectroscopic observations were performed between 2005 and 2008 in the framework of the CoRoT ground-based support campaign.

Our central finding is the discovery of the hybrid nature of the star: HD 49434 pulsates simultaneously in p- and g-modes. The frequency analysis shows clearly the presence of at least four γ Dor-type, as well as six δ Sct-type frequencies. Additional frequencies are expected to contribute to the observed variability, but have amplitudes close to or below our detection limit. All modes, for which an identification was possible, appear to be high-degree modes ($3 \leq \ell \leq 8$), which implies that future modelling will be extremely challenging.

The fairly rapid rotation of HD 49434 ($v_{\mathrm{eq}} \geq 87$ km s^{-1}) will also complicate modelling since the frequencies in the observers frame are rotationally modified with respect to those in the stellar rest frame. A high-degree, $m = -4$ mode could in fact shift the observed frequencies by 10 d^{-1}, which implies that a p-mode could appear with a typical g-mode frequency ($m < 0$) or vice-versa. We expect that the CoRoT time-series will provide additional information about the rotational frequency by the effects of rotational splitting. In this context, the frequency 2.666(2) d^{-1} might be interpreted as the rotational frequency f_{rot} of the star. Its first harmonic, 5.3311 d^{-1}, is detected in the line-profile variations, and if the f_{rot} value is confirmed, this could imply the presence of surface inhomogeneities. From the asymmetric behaviour of the amplitude distributions in the IPS diagrams (see Figs. 5 and 9), we found indications for local temperature variations on the stellar surface (Schrijvers & Telting 1999), but could not detect a clear periodicity in the corresponding EW variations. A similar behaviour was noted in other stars, such as the δ Sct star FG Vir (Zima et al. 2006) and the β Cep pulsator ε Cen (Schrijvers et al. 2004).

We encountered several puzzling results. For instance, it was not clear why we failed to detect the dominating frequency from the moment variations, 1.2732 d^{-1}, in the variations across the line profiles, and if this frequency could be linked with the photometric frequency 1.73480 d^{-1}. It was clear that the pulsational behaviour of HD 49434 is complex and that the rapid rotation adds to this complication. The simultaneous presence of several low-amplitude variations presented dificulties to the frequency search, which often resulted in an ambiguous determination of the frequency values (see Table 6). Moreover, some technical aspects of the analysis added to the confusion, such as the delicate process of the alignment of the data.

The detection of the hybrid nature of HD 49434 implies that it is an interesting asteroseismic target. The asteroseismic importance of hybrid γ Dor/δ Sct stars is obvious because both the envelope and the deep interior of the star can be probed by the study of p- and g-modes, respectively, providing a unique opportunity to constrain the macro-physics of the stellar interior. The amount of hybrid detections is steadily growing, although only a handful of cases is still known. The first discovery of its kind made was HD 209295 (A9/F0V, Handler et al. 2002). However, this primary of an eccentric binary might not be a bona fide hybrid variable because the excitation of its γ Dor-type variations is possibly induced by tidal interaction. To date, at least four other hybrid γ Dor/δ Sct stars have been reported, of which two were discovered from MOST satellite data: HD 8801 (A7m, Henry & Fekel 2005), HD 114839 (Am, King et al. 2006), BD+18 4914 (F5, Rowe et al. 2006), and HD 44195 (F0, Uytterhoeven et al. 2008). The simultaneous presence of p- and g-modes was also theoretically predicted (Dupret et al. 2004) and might not be as uncommon as it appears. Our results for HD 49434 indicate that the δ Sct-type modes have high degrees ($3 \leq \ell \leq 8$, see Table 7), and consequently are only detected in spectroscopic variations (Table 6) because high-degree modes cannot be detected in the integrated photometric light. This observational selection effect can explain why Handler & Shobbrook (2002), in their systematic survey for δ Sct variations in γ Dor stars using only photoelectric photometry, failed to detect hybrid variables other than

HD 209295. We can even speculate that a significant fraction of all γ Dor variables pulsate in both p- and g-modes, but the high-degree p-modes need spectroscopic detection. This finding would make the γ Dor pulsating class extremely suited for asteroseismic studies.

In a series of subsequent papers, we will confront the ground-based data, enlarged by a new spectroscopic time-series obtained in January/February 2008, with the actual CoRoT space data towards the goal of performing a deeper investigation and modelling of the star.

The combination of continuous and accurate space photometry, and ground-based spectroscopy promises to be the most robust way to study the frequency spectrum of HD 49434 in detail. Results from the analysis of data acquired by the MOST satellite indicate that not all high-degree spectroscopic modes can be recovered from photometric space data (e.g. ζ Oph, Walker et al. 2005), and consequently the spectroscopic observations will play an important part in the unraveling and understanding of the pulsational behaviour of the star.

The CoRoT satellite mission will provide an excellent opportunity to investigate the pulsational behaviour of a significant number of γ Dor variables, as, in the forthcoming years, continuous time-series of thousands of stars in the exo-planetary CCD field become available. Also, with at least two hybrid stars selected in the asteroseismic field of CoRoT, the target of this paper HD 49434, and HD 44195, we have good prospects of achieving progress in modelling and understanding the relation between p- and g-mode pulsators.

Acknowledgements. We thank Peter De Cat, Luciano Mantegazza, Wolfgang Zima and Andrea Miglio and the anonymous referee for useful comments on the first version of the paper. The FEROS data are being obtained as part of the ESO Large Programme: LP178.D-0361 (PI: Poretti). This work was supported by the italian ESS project, contract ASI/INAF I/015/07/0, WP 03170, by the Hungarian ESA PECS project No. 98022 and by the European Helio- and Asteroseismology Network (HELAS), a major international collaboration funded by the European Commission's Sixth Framework Programme. K.U. acknowledges financial support from a *European Community Marie Curie Intra-European Fellowship*, contract number MEIF-CT-2006-024476. P.J.A. acknowledges financial support from a Ramon y Cajal contract of the Spanish Ministry of Education and Science.

References

Aerts, C., De Pauw, M., & Waelkens, C. 1992, A&A, 266, 294
Asplund, M., Grevesse, N., & Sauval, A. J. 2005, in Cosmic Abundances as Records of Stellar Evolution and Nucleosynthesis in honor of David L. Lambert, ed. Th. G. Barnes III, & F. N. Bash, ASP Conf. Ser., 336, 25
Baglin, A., Auvergne, M., Boisnard, L., et al. 2006, in 36th COSPAR Scientific Assembly, 36, 3749
Bevington, P. R. 1969, Data reduction and error analysis for the physical sciences (New York: McGraw-Hill)
Breger, M., Stich, J., Garrido, R., et al. 1993, A&A, 271, 482
Briquet, M., & Aerts, C. 2003, A&AS, 398, 687
Bruntt, H., Catala, C., Garrido, R., et al. 2002, A&A, 389, 345
Bruntt, H., Bikmaev, I. F., Catala, C., et al. 2004, A&A, 425, 683
Catala, C., Poretti, E., Garrido, R., et al. 2006, in The CoRoT Mission, ed. M. Fridlung, A. Baglin, J. Lochard, & L. L. Conroy, ESA Spec. Publ., 1306, 329
Claret, A. 1995, A&AS, 109, 441
Donati, J.-F., Semel, M., Carter, B. D., Rees, D. E., & Collier Cameron, A. 1997, MNRAS, 291, 658
Donati, J.-F., Catala, C., Wade, G. A., et al. 1999, A&AS, 134, 149
Dupret, M.-A., Grigahcène, A., Garrido, R., Gabriel, M., & Scuflaire, R. 2004, A&A, 414, L17
Dupret, M.-A., Grigahcène, A., Garrido, R., Gabriel, M., & Scuflaire, R. 2005, A&A, 435, 927
Foster, G. 1995, AJ, 109, 1889
Gray, D. F. 2005, The observation and analysis of stellar photospheres (Cambridge: Cambridge University press)
Gillon, M., & Magain, P. 2006, A&A, 448, 341
Grevesse, N., & Sauval, A. J. 1998, Space Sci. Rev., 85, 161
Grigahcène, A., Dupret, M. A., Garrido, R., Gabriel, M., & Scuflaire, R. 2004, CoAst, 145, 10
Guzik, J. A., Kaye, A. B., Bradley, P. A., Cox, A. N., & Neuforge, C. 2000, ApJ, 542, L57
Handler, G., & Shobbrook, R. R. 2002, MNRAS, 333, 251
Handler, G., Balona, L. A., Shobbrook, R. R., et al. 2002, MNRAS, 333, 262
Hauck, B., & Mermilliod, M. 1998, A&AS, 129, 431
Hearnshaw, J. B., Barnes, S. I., Kershaw, G. M., et al. 2002, Exp. Astron., 13, 59
Henry, G. W., & Fekel, F. C. 2005, AJ, 129, 2026
Kaye, A. B., Handler, G., Krisciunas, K., Poretti, E., & Zerbi, F. M. 1999, PASP, 111, 840
King, H., Matthews, J. M., Rowe, J. F., et al. 2006, CoAst, 148, 28
Künzli, M., North, P., Kurucz, R. L., & Nicolet, B. 1997, A&AS, 122, 51
Kupka, F., & Bruntt, H. 2001, in First COROT/MONS/MOST Ground Support Workshop, 39
Kupka, F., Piskunov, N., Ryabchikova, T. A., Stempels, H. C., & Weiss, W. W. 1999, A&AS, 138, 119
Kurucz, R. L. 1993, ATLAS9, Stellar Atmosphere Programs, CD-ROM, 18, Smithonian Astrophysical Observatory
Kuschnig, R., Weiss, W. W., Gruber, R., et al. 1997, A&A, 328, 544
Lastennet, E., Lignieres, F., Buser, R., et al. 2001, A&A, 365, 535
Masana, E., Jordi, C., & Ribas, I. 2006, A&A, 450, 735
Mathias, P., Le Contel, J.-M., Chapellier, E., et al. 2004, A&A, 417, 189
Mermilliod, J.-C., Hauck, B., & Mermilliod, M. 1997, A&AS, 124, 349
Montgomery, M. H., & O'Donoghue, D. 1999, Delta Scuti Star Newsletter, 13, 28
Napiwotzki, R., Schoenberner, D., & Wenske, V. 1993, A&A, 268, 653
Perryman, M. A. C., Lindegren, L., Kovalevsky, J., et al. 1997, A&A, 323, L49
Piskunov, N. E., Kupka, F., Ryabchikova, T. A., Weiss, W. W., & Jeffery, C. S. 1995, A&AS, 112, 525
Poretti, E., & Zerbi, F. 1993, A&A, 268, 369
Poretti, E., Garrido, R., Amado, P. J., et al. 2003, A&A, 406, 203
Poretti, E., Alonso, R., Amado, P. J., et al. 2005, AJ, 129, 2461
Rainer, M. 2003, Analisi spettrofotometriche di stelle da usare come targets per la missione spaziale CoRoT, Laurea Thesis, Universitá degli Studi di Milano
Rowe, J. F., Matthews, J. M., Cameron, C., et al. 2006, CoAst, 148, 34
Ryabchikova, T. A., Piskunov, N. E., Stempels, H. C., Kupka, F., & Weiss, W. W. 1999, Physica Scripta, 83, 162
Sbordone, L. 2005, MSAIS, 8, 61
Scargle, J. D. 1982, ApJ, 263, 835
Schrijvers, C., & Telting, J. H. 1999, A&A, 342, 453
Schrijvers, C., Telting, J. H., & Aerts, C. 2004, A&A, 416, 1069
Skuljan, J. 2004, in Variable Stars in the Local Group, ed. D. W. Kurtz, & K. R. Pollard, ASP Conf. Ser., 188, IAU, 193, 575
Stellingwerf, R. F. 1978, ApJ, 224, 953
Takeda, Y. 1995, PASJ, 47, 287
Telting, J. H., & Schrijvers, C. 1997, A&A, 317, 723
Townsend, R. H. D. 1997, MNRAS, 284, 839
Uytterhoeven, K., Briquet, M., Aerts, C., et al. 2004, A&A, 432, 955
Uytterhoeven, K., Poretti, E., & the CoRoT SGBOWG 2007, CoAst, 150, 371
Uytterhoeven, K., Poretti, E., Rainer, M., et al. 2008, in HelasII international conference: Helioseismology, Asteroseismology and MHD Connections, J. Phys.: Conf. Ser., IOP Publishing, in press [arXiv:0710.4068]
Vaníček, P. 1971, Ap&SS, 12, 10
Walker, G. A. H., Kuschnig, R., Matthews, J. M., et al. 2005, ApJ, 623, L145
Zima, W., Wright, D., Bentley, J., et al. 2006, A&A, 455, 235

Table 1. Journal of the photometric observations of HD 49434.

Date	JD	# Data points			Date	JD	# Data points			Date	JD	# Data points		
		SNO	SPMO	KO			SNO	SPMO	KO			SNO	SPMO	KO
21 Mar. 2003	2720.2	...	...	4	03 Mar. 2006	3798.4	13	...	...	13 Mar. 2007	4173.3	9	...	...
22 Mar. 2003	2721.2	...	...	7	06 Mar. 2006	3801.4	7	...	...	17 Mar. 2007	4177.3	16	...	...
23 Mar. 2003	2722.2	...	...	7	07 Mar. 2006	3802.3	17	...	...	18 Mar. 2007	4178.3	9	...	...
24 Mar. 2003	2723.2	...	...	7	08 Mar. 2006	3803.3	10	...	...	22 Mar. 2007	4182.3	15	...	...
25 Mar. 2003	2724.2	...	...	6	10 Nov. 2006	4049.5	30	...	...	15 Nov. 2007	5519.6	20	...	...
20 Jan. 2005	3391.3	32	...	...	11 Nov. 2006	4050.5	25	...	...	16 Nov. 2007	5520.5	25	...	...
21 Jan. 2005	3392.3	57	...	...	12 Nov. 2006	4051.5	32	...	...	17 Nov. 2007	5521.5	21	...	...
22 Jan. 2005	3393.3	59	...	...	13 Nov. 2006	4052.5	32	...	...	28 Nov. 2007	5533.4	39	...	...
12 Nov. 2005	3686.7	...	16	...	14 Nov. 2006	4053.5	36	...	...	30 Nov. 2007	5535.4	39	...	...
13 Nov. 2005	3687.7	...	22	...	15 Nov. 2006	4054.6	17	...	...	02 Dec. 2007	5537.4	12	...	...
14 Nov. 2005	3688.7	...	25	...	18 Nov. 2006	4057.6	15	...	...	03 Dec. 2007	4437.8	...	19	...
15 Nov. 2005	3689.7	...	23	...	20 Nov. 2006	4059.6	21	23	...	04 Dec. 2007	4438.6	12	27	...
06 Dec. 2005	3711.4	26	...	...	21 Nov. 2006	4060.6	9	17	...	05 Dec. 2007	4439.6	14	28	...
07 Dec. 2005	3712.4	31	...	...	22 Nov. 2006	4061.8	...	18	...	06 Dec. 2007	4440.6	12	22	...
12 Dec. 2005	3717.4	10	...	...	23 Nov. 2006	4062.6	18	9	...	07 Dec. 2007	4441.9	...	7	...
13 Dec. 2005	3718.4	8	...	...	24 Nov. 2006	4063.6	13	16	...	08 Dec. 2007	4442.8	...	5	...
14 Dec. 2005	3719.4	10	...	...	26 Nov. 2006	4065.7	...	15	...	10 Dec. 2007	4444.6	18	...	...
15 Dec. 2005	3720.4	9	...	...	27 Nov. 2006	4066.7	...	13	...	11 Dec. 2007	4445.6	14	...	...
17 Dec. 2005	3722.4	11	...	...	28 Nov. 2006	4067.7	...	22	...	12 Dec. 2007	4446.6	10	...	...
18 Dec. 2005	3723.4	5	...	...	29 Nov. 2006	4068.7	...	30	...	13 Dec. 2007	4447.7	...	25	...
20 Dec. 2005	3725.4	26	...	...	30 Nov. 2006	4069.7	...	20	...	14 Dec. 2007	4448.8	...	16	...
21 Dec. 2005	3726.3	49	...	...	01 Dec. 2006	4070.7	...	30	...	15 Dec. 2007	4449.8	...	16	...
22 Dec. 2005	3727.4	20	...	...	02 Dec. 2006	4071.7	...	31	...	29 Dec. 2007	4463.6	10	...	...
02 Jan. 2006	3738.4	11	...	...	03 Dec. 2006	4072.7	...	28	...	31 Dec. 2007	4465.6	12	...	...
04 Jan. 2006	3740.4	14	...	...	04 Dec. 2006	4073.7	...	25	...	10 Jan. 2008	4476.4	33	...	...
11 Jan. 2006	3747.3	20	...	...	05 Dec. 2006	4074.7	...	25	...	12 Jan. 2008	4478.3	42	...	...
01 Feb. 2006	3768.3	33	...	...	06 Dec. 2006	4075.7	...	28	...	18 Jan. 2008	4484.4	35	...	...
04 Feb. 2006	3771.3	47	...	...	24 Jan. 2007	4125.3	44	...	...	19 Jan. 2008	4485.3	37	...	...
27 Feb. 2006	3794.4	12	...	...	26 Feb. 2007	4158.3	15	...	...	20 Jan. 2008	4486.3	37	...	...
01 Mar. 2006	3796.4	15	...	...	11 Mar. 2007	4171.3	12	...	...	...	...	...	...	...

Julian Dates are given with respect to $JD_0 = 2\,450\,000$.

Table 3. Journal of the spectroscopic observations of HD 49434.

FEROS			SOPHIE			FOCES		
date	JD	# spectra	date	JD	# spectra	date	JD	# spectra
03 Jan. 2007	4103.7	5	11 Jan. 2007	4112.4	22	04 Dec. 2006	4074.4	50
04 Jan. 2007	4104.6	7	12 Jan. 2007	4113.4	30	...	...	...
05 Jan. 2007	4105.6	6	13 Jan. 2007	4114.4	40	...	...	...
06 Jan. 2007	4106.6	5	14 Jan. 2007	4115.4	30	HERCULES		
07 Jan. 2007	4107.6	5	15 Jan. 2007	4116.4	18	date	JD	# spectra
08 Jan. 2007	4108.6	6	17 Jan. 2007	4118.4	19	01 Feb. 2007	4132.9	6
09 Jan. 2007	4109.5	8	18 Jan. 2007	4119.4	13	04 Feb. 2007	4135.9	19
10 Jan. 2007	4110.5	7	19 Jan. 2007	4120.4	24	05 Feb. 2007	136.9	23
11 Jan. 2007	4111.6	5	20 Jan. 2007	4121.4	23	06 Feb. 2007	4137.9	26
25 Jan. 2007	4125.6	3	27 Jan. 2007	4128.3	31	12 Feb. 2007	4143.9	11
26 Jan. 2007	4126.6	4	28 Jan. 2007	4129.3	36	13 Feb. 2007	4144.9	22
27 Jan. 2007	4127.6	5	29 Jan. 2007	4130.3	41	14 Feb. 2007	4145.9	28
28 Jan. 2007	4128.6	5	30 Jan. 2007	4131.3	42	16 Feb. 2007	4147.9	30
29 Jan. 2007	4129.7	2	31 Jan. 2007	4132.3	41	17 Feb. 2007	4148.9	29

Julian Dates are given with respect to $JD_0 = 2\,450\,000$.

Table 9. The influence of changes in $T_{\rm eff}$, $\log g$, and microturbulence on the derived average LTE abundances, $\log \epsilon(N)$, of HD 49434.

$T_{\rm eff}$ (K)	7300		7700		6900		7300		7300		7300		7300	
$\log g$ (dex)	4.20		4.20		4.20		4.10		4.30		4.20		4.20	
ξ (km s^{-1})	2		2		2		2		2		1		3	
$v \sin i$	89 ± 3		89 ± 3		90 ± 3		89 ± 3		89 ± 3		89 ± 3		89 ± 3	
C	8.70	0.14	8.79	0.11	8.79	0.17	8.69	0.15	8.73	0.15	8.48	0.52	8.68	0.22
O	8.86	…	8.65	…	9.11	…	8.83	…	8.89	…	8.84	…	8.85	…
Na	6.02	…	6.21	…	5.84	…	6.05	…	5.97	…	6.35	…	5.76	…
Mg	7.67	0.09	8.02	0.08	7.26	0.06	7.75	0.06	7.63	0.09	7.95	0.34	7.62	0.38
Si	7.52	0.47	7.58	0.37	7.25	0.42	7.55	0.27	7.53	0.28	7.37	0.62	7.46	0.45
S	7.31	…	7.53	…	7.74	…	7.30	…	7.33	…	7.16	…	7.21	…
Ca	6.60	0.16	6.70	0.14	6.38	0.13	6.62	0.07	6.65	0.10	6.77	0.57	6.48	0.16
Sc	3.52	0.28	3.60	0.17	3.53	0.24	3.45	0.20	3.53	0.21	4.18	0.89	3.35	0.26
Ti	5.10	0.22	5.21	0.21	4.83	0.25	4.97	0.21	5.03	0.23	4.85	0.82	4.94	0.22
V	4.25	0.30	4.65	…	4.45	…	4.53	…	4.56	…	4.38	…	4.18	…
Cr	5.87	0.23	6.05	0.18	5.72	0.19	5.89	0.24	5.90	0.27	5.87	0.51	5.79	0.22
Mn	5.37	0.35	5.68	0.18	5.07	0.40	5.44	0.18	5.44	0.19	5.32	0.96	5.41	0.39
Fe	7.50	0.12	7.70	0.10	7.29	0.11	7.49	0.11	7.49	0.11	7.40	0.38	7.39	0.10
Co	5.34	…	5.53	…	…	…	5.33	…	5.35	…	4.65	…	5.36	…
Ni	6.23	0.16	6.49	0.16	6.13	0.15	6.30	0.17	6.30	0.17	6.25	0.37	6.24	0.24
Cu	4.03	…	4.12	…	3.79	…	4.03	…	4.03	…	3.91	0.11	4.07	0.08
Y	2.51	0.18	2.68	0.17	2.32	0.25	2.49	0.18	2.54	0.19	2.03	0.31	2.43	0.38
Zr	2.74	0.15	2.98	…	2.79	…	2.53	…	2.84	…	2.78	2.30	0.71	…
Ba	3.24	0.06	3.47	…	2.89	…	3.21	0.02	3.21	0.02	3.81	0.07	2.58	0.10
La	1.17	…	1.56	…	0.93	…	1.16	…	1.17	…	0.89	…	…	…
Ce	2.13	…	2.30	…	1.84	…	2.07	…	2.20	…	2.08	…	1.73	…
Nd	1.18	…	…	…	…	…	1.13	…	1.27	…	…	…	…	…